Sol-gel-derived glass scaffold with high pore interconnectivity and enhanced bioactivity

Ana C. Marques[a] and Rui M. Almeida
Departamento de Engenharia de Materiais/Instituto de Ciência e Engenharia de Materiais e Superfícies (ICEMS), Instituto Superior Técnico/TULisbon, 1049-001 Lisboa, Portugal

Amath Thiema[b]
International Materials Institute for New Functionality in Glass, Lehigh University, Bethlehem, PA 18015

Shaojie Wang
Department of Materials Science and Engineering, Lehigh University, Bethlehem, Pennsylvania 18015

Matthias M. Falk
Department of Biological Sciences, Lehigh University, Bethlehem, Pennsylvania 18015

Himanshu Jain[c]
Department of Materials Science and Engineering, Lehigh University, Bethlehem, Pennsylvania 18015

(Received 1 June 2009; accepted 14 July 2009)

We report on the preparation of a bioactive $CaO–SiO_2$ monolithic scaffold with interconnected bimodal nanomacro porosity, which simulates the morphology of a natural trabecular bone, by a newly developed modified sol-gel process. This method inherently creates nanopores, whose average diameter can be tailored to approximately 5–20 nm by solvent exchange. To achieve interconnected macroporosity (pores ~5–300 μm in size), a polymer [poly(ethylene oxide)] is added, which causes phase separation simultaneously with the sol-gel transition. High-resolution scanning electron microscopy and mercury intrusion porosimetry demonstrate a high degree of three-dimensional interconnectivity and sharp distributions of pore size. In vitro bioactivity tests in simulated body fluid (SBF) show bioactivity of the material after soaking for approximately 5 h, as verified by the formation of a hydroxyapatite layer deep into the scaffold structure. Analysis of the SBF after the reaction indicates the dissolution of the samples, another desired feature of temporary scaffolds for bone regeneration. MG63 osteoblast-like cells seeded on our sol-gel glass samples responded better to samples with nanopores enlarged by a solvent exchange process than to the one with normal nanopores. Thus, the benefits of the high surface area achieved by sol-gel and solvent exchange procedures are most clearly demonstrated for the first time.

I. INTRODUCTION

Cell-based tissue engineering using the patient's own cells cultured in a biomaterial scaffold represents a promising therapy for bone regeneration, but there is still lack of a clinically efficient scaffold. One of its desired features, in addition to bioactivity, is the bonelike morphology that consists of nano- and macroporosities simultaneously. Unfortunately, thermodynamics make the coexistence of nanopores and macropores unstable under equilibrium conditions, as the larger pores tend to absorb the smaller ones. This work describes the preparation of a $SiO_2–CaO$ monolithic scaffold based on a modified sol-gel process, which circumvents these thermodynamic predictions.

Gel-derived glasses in the $SiO_2–CaO$ system are categorized as bioactive glasses[1] since they develop an apatite-like layer when soaked in simulated body fluid (SBF)—a solution similar to the human blood plasma. This layer is at the origin of the bond formed between bioactive materials and living tissues.[2] Bioactive glasses with hierarchical porosity, having interconnected pores in the nano- and macro-size ranges, have the advantage of simultaneously exhibiting high surface area and, therefore, rapid crystallization of hydroxyapatite (HA)[3] plus cell adhesion, due to the nanopores (~5–50 nm), as suggested

[a]Present address: Surface & Interface Solutions Center, Dow Corning Europe S.A., B-7180 Seneffe, Belgium.
[b]Permanent address: Department of Physics, University Cheikh Anta Diop de Dakar, Dakar, Senegal.
[c]Address all correspondence to this author.
e-mail: hj00@lehigh.edu
This author was an editor of this journal during the review and decision stage. For the *JMR* policy on review and publication of manuscripts authored by editors, please refer to http://www.mrs.org/jmr_policy
DOI: 10.1557/JMR.2009.0440

in Ref. 3 and shown in this work, combined with increased nutrient and excretory substance transport[4] and tissue ingrowth, due to the macropores (in excess of 100 μm).

Sol-gel-derived bioactive glasses exhibit a high specific surface area, high osteoconductive properties, significant degradability, and also an inherent nanoporosity (normally below 10 nm), so that the principal challenge lies in introducing macropores larger than 100 μm. Samples that were both nanoporous (~2–10 nm pores) and macroporous (~0.1–40 μm pores) have been fabricated on the basis of polymerization-induced phase separation in various silica-based sol-gel systems by using organic polymers such as poly(ethylene oxide) (PEO), poly(ethylene glycol) (PEG), or poly(acrylic acid) (PAA),[5,6] with no evidence of bioactivity or biocompatibility. Sepulveda et al.[7] and, more recently, Jones et al.[8] have reported the preparation of macroporous matrices (pores >100 μm) by foaming sol-gel systems where a surfactant (e.g., Teepol) was added to a sol prepared from a mixture of alkoxides, deionized water, and HNO_3.[8] Other possible techniques to create macroporosity in materials are (i) Chmelka's method,[9] where macroporous templates such as a polystyrene foam or an oil-in-water emulsion are used; or (ii) the salt sintering process,[10] where a glass prepared by melt quenching is crushed and mixed with sodium chloride, followed by heat treatment and final immersion in water to promote dissolution of the salt. More recently, hierarchically three-dimensional (3-D) mesoporous-macroporous bioactive glasses were prepared using a combination of sol-gel, evaporation-induced self-assembly, and multipolymer templating processes.[11] Unfortunately, the mechanical properties of most of today's available porous scaffolds fall short of those exhibited by complex human tissues such as bone and ligament. However, the coral-like morphology (with interconnected macropores) formed during phase separation by spinodal decomposition (the technique used in the present work) might lead to mechanically stronger materials than those obtained by foaming, fugitive phase burnout,[12] or dissolution, where high pore volumes are required for the interconnection of the (spherelike) pores.

This work reports on the preparation and characterization of texture, morphology, in vitro bioactivity, and resorbability of nano/macroporous bioactive gels/glasses for scaffolds with optimum porosity for bone regeneration. The preparation method is based on the polymerization-induced (spinodal-type) phase separation, which is accomplished in parallel with the sol-gel transition.

II. MATERIALS AND METHODS

A. Scaffold preparation and characterization

A silica-based bioactive composition (70% SiO_2–30% CaO) was synthesized using the sol-gel/phase separation technique, where interconnected macroporosity is formed by inducing spinodal decomposition of a gelling sol to occur simultaneously with the sol-gel transition, as already described in Refs. 13 and 14.

First, a water soluble polymer (PEO, with an average molecular weight, M_w ~100,000) was dissolved in 0.05 N acetic acid (CH_3COOH) aqueous solution, to which 9 mL of tetramethoxysilane (TMOS) were added (1.4 g of PEO to 9 mL of TMOS). Calcium nitrate tetrahydrate, $Ca(NO_3)_2{\cdot}4H_2O$ was then added and gelation was allowed to occur at 40 °C, after adding 2 mL of deionized (DI) water and a few drops of HF. The gel was aged at room temperature (RT), for 1 day. Solvent exchange was then performed by immersing the well-aged gel, still in the wet state, in DI water at RT for 3 h and then in ammonia (NH_4OH) aqueous solution for 1 day, at 40 °C. The resulting gels were dried at 60, 120, and 150 °C and sintered sequentially at 600 °C (1 h) and 700 °C (2 h). Samples were also prepared without a polymer and/or solvent exchange procedure for comparison.

The pore morphology and textural features of the heat-treated samples (coated with iridium) were observed by field-emission scanning electron microscopy (FE-SEM) (Hitachi 4300, Pleasanton, CA), in the secondary electron mode, at 5 kV. The interconnected pore size for the scaffolds prepared in this work, as well as the volume fraction of porosity and density, were measured by mercury intrusion porosimetry (Autopore IV, Micromeritics Co., Norcross, GA).

Thermal analysis of the samples was conducted using a differential thermal analysis (DTA)/thermogravimetric analysis (TGA) instrument (Netzsch STA 409, Selb, Germany) for monitoring the reactions responsible for the formation of nano- and macropores in the samples.

B. Dissolution and bioactivity tests

The examination of apatite formation on the surface of a material in SBF has been proven useful for predicting the in vivo bone bioactivity of a material,[15] leading to a remarkable reduction in the number of animals used for in vivo experiments, as well as the duration of such experiments. SBF was the aqueous medium used in this work for the in vitro dissolution and bioactivity tests. It was prepared following the recipe described in Ref. 7 taking into account the notes included in Ref. 15.

Previously weighed pieces of the porous material were soaked in SBF (0.01 g of sample per mL of SBF), at pH = 7.40 and 36.5 °C, for selected periods of time up to 5 days, under slow stirring at ~1 Hz (to avoid that homogeneously precipitated HA in SBF might deposit on the sample). The samples were removed from the SBF and rinsed with acetone to terminate any on-going reaction and were then characterized by SEM [with energy dispersive x-ray spectrometry (EDX)]. Diffuse reflectance infrared Fourier transform spectra (DRIFTS) were also collected, using a Nicolet 5700 FTIR spectrometer

(Thermo Fisher Scientific Inc., Waltham, MA), in the range of 350 to 1500 cm^{-1}. DRIFTS samples were prepared by scrapping off the surface layer of the scaffolds and grinding it together with KBr (sample to KBr mass ratio of 1:10) to avoid specular reflectance.

SBF extracts after reaction, obtained by filtration (1-μm paper), were analyzed by inductively coupled plasma spectroscopy (ICP model: Perkin-Elmer OPTIMA 2100 DV, Waltham, MA), to determine the Si, P, and Ca concentrations in solution.

C. In vitro cell response test

MG63 osteoblast-like cells (ATCC, CRL-1427) were chosen as the model to study cell response to our samples. The cells were cultured in a 6-cm tissue culture dish and maintained in an incubator at a temperature of 37 °C regulated with 5% CO_2, 95% air, and a saturated humidity. Dulbecco's Modified Eagle Medium (DMEM) supplemented with 10% fetal bovine serum (FBS) and 1% penicillin/streptomycin was used as the complete culture medium. The cells were subcultured at confluence.

Before cell seeding, the samples were soaked in 70% ethanol and then in water for 5 min, respectively, air dried, sterilized under ultraviolet (UV) for 10 min, and presoaked in complete culture medium for 30 min. Cells were then harvested from the tissue culture dish and seeded on the sol-gel glass samples containing no macropores, prepared with and without solvent exchange. Their morphology was observed after 40 h of exposure to the glass surface.

For SEM imaging, samples were removed from tissue culture plates and the cells were rinsed in 0.1 M phosphate buffer solution, fixed in a 0.1 M phosphate buffer with 3% glutaraldehyde (w/v), rinsed in a 0.1 M phosphate buffer, stepwise dehydrated in graded series of ethanol (35%, 60%, 80%, 95%, 95%, and 100%), dried using hexamethyldisilazane (HMDS, Sigma, St. Louis, MO), iridium-sputter coated with a 5-nm-thick coating, and examined using a Philips XL-30 SEM (Hillsboro, OR) at an accelerating voltage of 5 kV.

III. RESULTS AND DISCUSSION

A. Scaffold characterization

Figure 1 shows the SEM micrographs of a SiO_2–CaO glass sample obtained by two different techniques assessed in this study: the conventional sol-gel method and the sol-gel/phase separation technique with the addition of PEO, respectively. The latter technique leads to novel scaffolds obtained in this work [Fig. 1(b)], which exhibit a macroporous network, in contrast with the structure of Fig. 1(a) for samples prepared without polymer, where no pores are revealed at the given magnification. Both samples were prepared with solvent exchange.

Figure 2(a) is a higher magnification image of Fig. 1(b), showing the interconnected macroporous network with pores of ~5–300 μm in size within a coral-like skeleton. Figure 2(b) reveals the nanotexture of such scaffold at the highest magnification.

The samples prepared in this work by the sol-gel/phase separation technique with the addition of PEO polymer, and subsequent solvent exchange procedure are, therefore, found to present a multimodal pore size distribution with nanopores of ~5 to 20 nm in size and macropores from ~5 to 300 μm in size. These pores are largely interconnected within a coral-like or wormlike morphology, resulting from phase separation by spinodal decomposition. A comprehensive study of the morphology and microstructure of these materials has been recently reported in Ref. 14. The total pore area is as large as 423 m^2/g with a volume fraction of porosity at 61%, which is found to be lower than the typical value for scaffolds with spherical pores (80–90%). Thus, it is demonstrated that the pore volume, which lowers mechanical strength, does not need to be large to yield

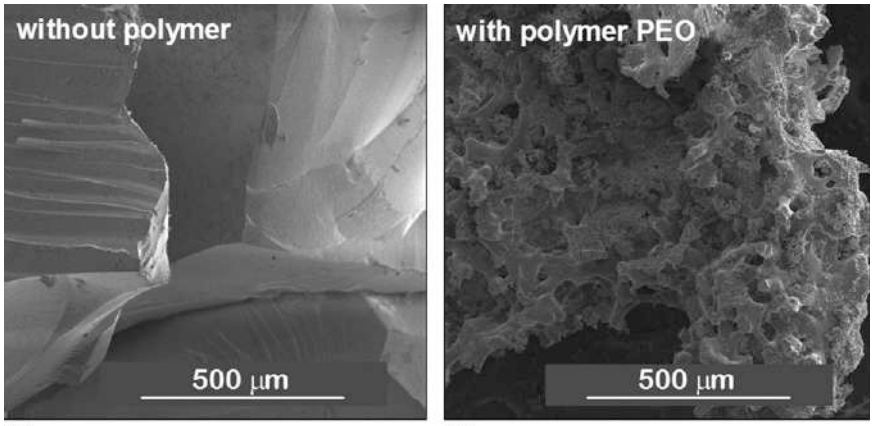

FIG. 1. SEM micrographs of heat-treated scaffold samples of composition 70 SiO_2–30 CaO (mol%), prepared by (a) the sol-gel technique without addition of polymer; (b) the sol-gel/phase separation technique with addition of PEO.

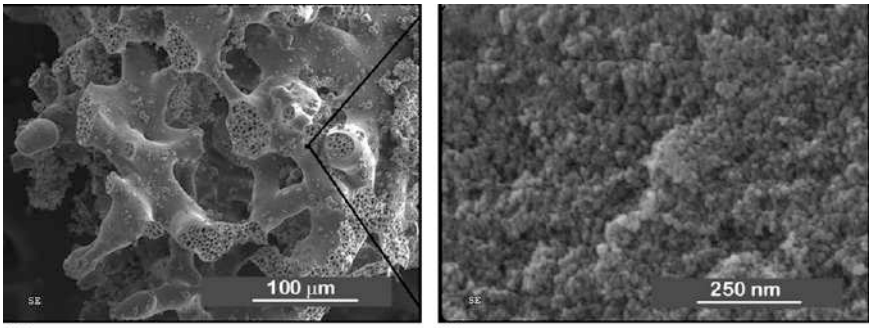

FIG. 2. SEM micrographs of a heat-treated scaffold of composition 70 SiO_2–30 CaO (mol%), prepared by the sol-gel/phase separation technique with addition of PEO: (a) magnification of 300×; (b) magnification of 120,000×.

interconnected macropores—a clear advantage over the scaffolds made with spherical pores.[8,10]

The pore interconnectivity of the scaffolds is evidenced in the micrographs of Figs. 1(b) and 2(a), where large pore necks are observed; the pore interconnectivity exhibited by these samples together with their nanotexture is a further advantage with regard to dissolution and bioactivity, which is essential for bone scaffolding applications. Moreover, the progressive dissolution of the scaffolds can promote even more interconnectivity due to the rupture of thin walls between isolated pores.

Figure 3 shows the pore size distribution curve obtained from mercury porosimetry on a 70% SiO_2–30% CaO scaffold prepared with polymer PEO, with and without solvent exchange and for a sample of the same composition prepared without polymer, but after solvent exchange. The peak macropore size for the scaffold prepared with PEO was around 60 μm and it ranged from ~5 to 300 μm, whereas the sample prepared without polymer did not present any measurable amount of macropores. Nanopores were found to be ~10 nm in size for samples prepared with solvent exchange and smaller for the scaffold without solvent exchange, with the peak nanopore size below the detection limit by Hg porosimetry (5 nm). Although the identification of small mesopores by Hg intrusion at high pressure is questionable, these results have been confirmed by independent N_2 adsorption Brunauer–Emmett–Teller (BET) analysis, not shown in this work.

Solvent exchange increases the nanoporosity,[13] leading to a larger nanopore peak size, as shown in Fig. 3 (e.g., at 10 nm versus <5 nm without solvent exchange). Note that the nanopore sizes can be increased systematically by using longer solvent exchange periods and/or using a more concentrated NH_4OH aqueous solution. Silica is known to exhibit appreciable solubility at high pH. Therefore, when the wet gels are soaked in ammonia aqueous solution (pH~10), the pore structure evolution is thought to be driven by a coarsening of particles in the gel, through dissolution-reprecipitation of the fractally rough surface of the silica gel network,[5] leading to an

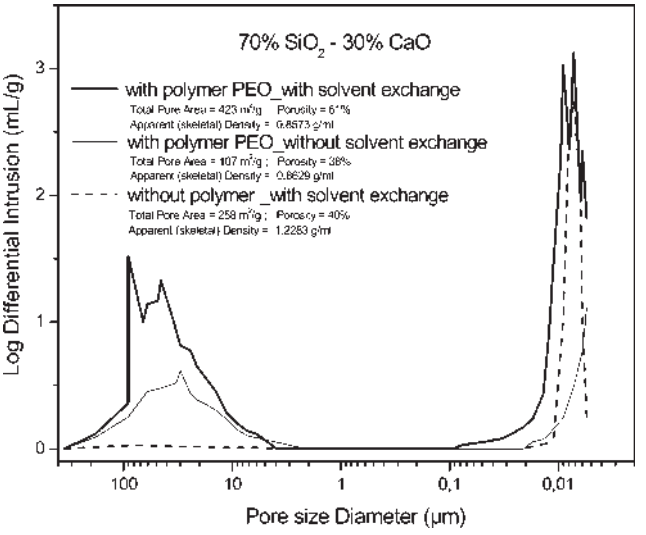

FIG. 3. Interconnected pore size distributions for heat treated scaffolds of composition 70 SiO_2–30 CaO (mol%), determined by mercury intrusion porosimetry. The scaffolds analyzed were prepared both with and without PEO, as well as with and without solvent exchange.

enlargement of the nanopore size. Indeed, with solvent exchange an increase in total pore area from 107 to 423 m^2/g and in volume fraction of porosity from 38% to 61% is observed (caption, Fig. 3). On the other hand, macroporosity was reported in previous works as being dependent on the inorganic precursors/polymer molar ratio, the gelation temperature, and the catalyst content.[5,12] We find that the increase of polymer concentration, gelation temperature and/or the hydrolysis catalyst content causes phase separation after the sol-gel transition, which results in finer domains and correspondingly smaller macropore size. The presence of polymer may also play a role in the broadening of the nanopore size distribution, as observed in Fig. 3. Finally, it is worth noting that the pore morphology observed in SEM and x-ray micrographs is in excellent agreement with the results of Hg porosimetry.

Figure 4 shows the pore size distribution, in a 70% SiO_2–30% CaO scaffold prepared with PEO and solvent

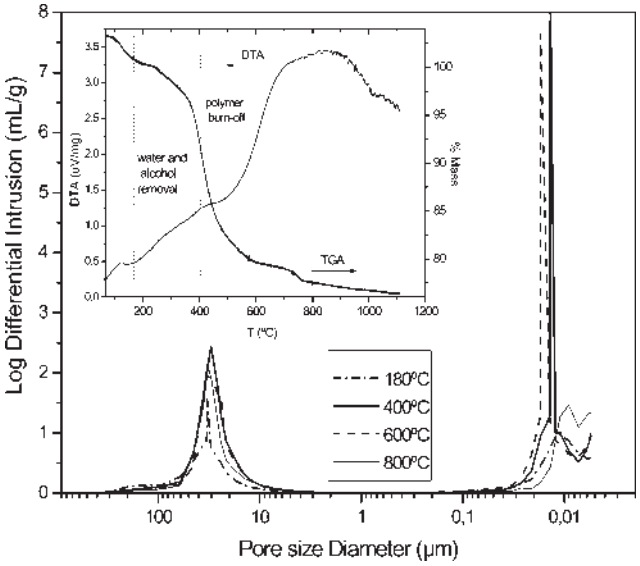

FIG. 4. Pore size distribution in a 70 SiO_2–30 CaO (mol%) scaffold, for different heat-treatment temperatures up to 800 °C, for 1 h. The inset shows corresponding DTA and TGA curves.

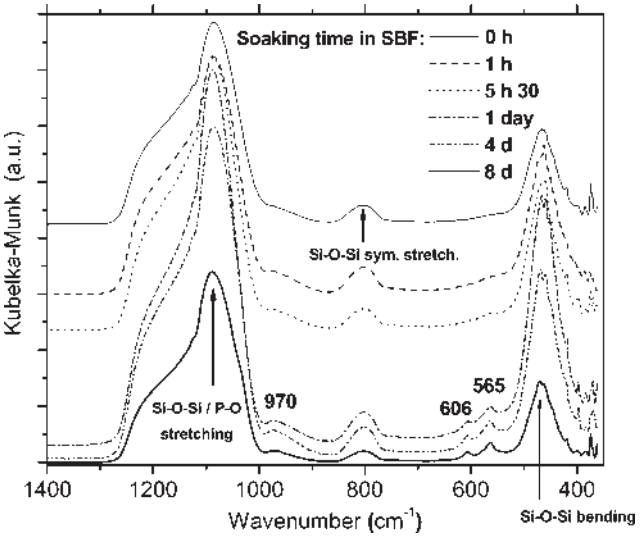

FIG. 5. Evolution of DRIFTS spectra for 70 SiO_2–30 CaO (mol%) scaffolds soaked in SBF for selected periods of time, up to 8 days. The spectrum corresponding to the same scaffold with no exposure to SBF is also shown for comparison.

exchange, for different heat-treatment temperatures up to 800 °C and the inset shows DTA and TGA graphs of the same scaffold, dried at 60 °C, but not heat treated.

DTA measures temperature changes associated with absorption or release of heat energy, whereas TGA gives simultaneous mass change in the system. The poor quality of the baseline in the DTA trace allows us only to discern confidently an endothermic peak at ~180 °C, starting at ~110 °C. It is ascribed to water and solvent removal such as alcohol by-products from polycondensation reactions, which typically form during sol-gel processing. There is also an exothermic peak at ~400 °C corresponding to PEO polymer burn-off, which is not present in the DTA trace of a sample prepared without the polymer (data not shown). These reactions are in accordance with the weight losses observed in the TGA trace. After the heat treatment at 180 °C, there is already a bimodal pore size distribution composed of macro- and nanopores, but it is after the heat treatment at 400 °C that a significant increase in the amount of macropores (and also nanopores) occurs. Therefore, water removal and polymer burn-off are both responsible for nano- and macroporosity formation, with water/solvent evaporation playing a more important role in the establishment of nanoporosity. Finally, heat treatments at significantly higher temperatures such as 800 °C lead to the elimination of a significant fraction of macro- and nanopores, typical of the densification at elevated temperatures.

B. Dissolution, bioactivity, and in vitro cell tests

The present dissolution and bioactivity tests have followed the Kokubo protocol,[7,15] keeping constant the ratio of sample mass to SBF volume, since different samples have been compared, with and without pores, rather than samples with different types of pores, for which a constant sample surface area to SBF volume might be preferable.

The DRIFTS spectra corresponding to 70% SiO_2–30% CaO scaffold also prepared with PEO and solvent exchange, left in SBF for different soaking times, including one not exposed to SBF for reference, are shown in Fig. 5. In this case, the diffuse reflectance values are transformed into Kubelka-Munk units (K/S), i.e., the ratios between the absorption coefficient (K) and the scattering coefficient (S) of the sample at any given wavelength, proportional to species concentrations. This has the advantage of easily following the increase in the concentration of the material deposited at the surface of the scaffold with increasing soaking time.

The IR spectra in Fig. 5 represent typical bands of a silicate glass network, common to all samples analyzed; the presence of CaO does not seem to make appreciable changes perhaps due to a poor incorporation of CaO into the SiO_2 structure. We observe a dominant band at about 1070 cm^{-1}, due to the asymmetric stretching of the Si–O–Si linkage, a weaker peak on its low-frequency side at ~970 cm^{-1}, due to Si–OH stretching vibrations, which is more intense after soaking in SBF, a peak at 800 cm^{-1} ascribed to symmetric stretching of the Si–O–Si bonding linkages, and a band at 470 cm^{-1} due to Si–O–Si bending movements.[16] The presence of peaks at 565 and 606 cm^{-1}, for samples exposed to SBF during at least 1 day, corresponds to O–P–O bending vibrations of PO_4^{3-} tetrahedra in crystalline calcium phosphate,[17] which suggests the formation of an HA layer or a layer of a similar composition with the immersion in SBF.

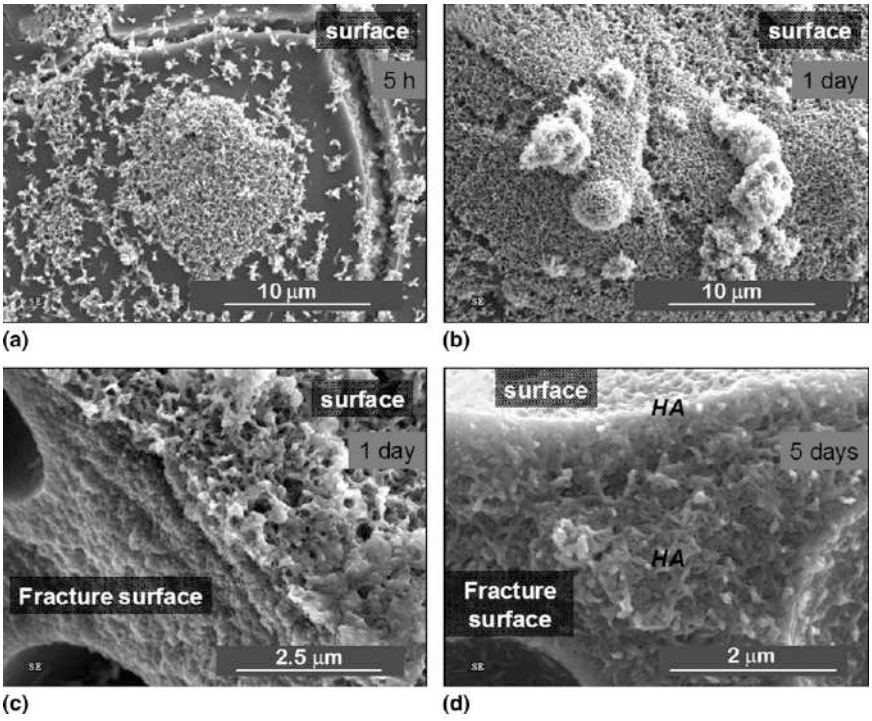

FIG. 6. SEM micrographs of a heat-treated scaffold of composition 70 SiO_2–30 CaO (mol%), prepared by the sol-gel/phase separation technique after exposure to SBF for selected periods of time: (a) 5 h, (b) 1 day, (c) 1 day, and (d) 5 days.

Figure 6 shows several SEM micrographs of the surface exposed to SBF and the cross section (fracture surface) of scaffolds immersed in SBF for 5 h, 1 day, and 5 days, which exhibit the progressive formation of a continuous layer at the surface, with the same characteristic features of apatite grains and layers. In Fig. 6(a), after 5 h of immersion in SBF, the formation of some clusters at the surface of the scaffolds is visible and, after 1 day in SBF [Figs. 6(b) and 6(c)] a continuous layer with morphology/structure typical of that of apatite or hydroxyapatite is visible as well. After 5 days of soaking in SBF, such HA-like structure is found not only at the surface, in the form of a thicker layer, but also inside the scaffold, as observed in the fractured cross section of the sample [Fig. 6(d)]. Besides HA formation on the surface directly exposed to SBF, there was also HA precipitation in the not "directly" exposed interior. The interconnectivity of the pores, revealed in Figs. 1(b) and 2, allows SBF to penetrate the interior of the scaffold, thus leading to the formation of HA not only at the surface, as it is found to happen in most of the published literature, but also throughout the 3-D scaffold structure. This type of HA formation will promote bone cell ingrowth, since adhesion and propagation of osteoblasts are known to be enhanced on a HA-rich surface.[18]

The micrograph of Fig. 7 corresponds to the sample prepared without polymer, after being soaked for 1 day in SBF. The structure at the surface consists of a discontinuous layer of a few plates.

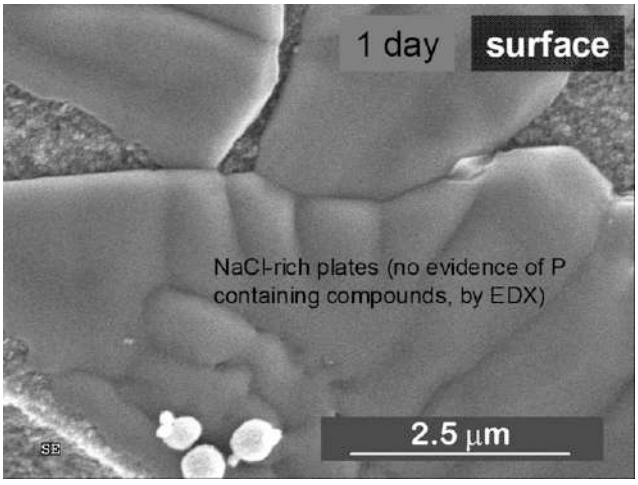

FIG. 7. SEM micrograph of a heat-treated scaffold of composition 70 SiO_2–30 CaO (mol%) after exposure to SBF for 1 day, prepared by the conventional sol-gel method (without addition of polymer) and, therefore, without macropores.

Comparing the micrograph of Fig. 6(c) with that of Fig. 7, we find a significant difference in terms of structure and composition of the surfaces of the samples prepared with and without the polymer. Unlike the sample prepared by our novel fabrication method using PEO polymer, the sample prepared without the polymer shows no macropores and smaller nanopores. It also does not show HA formation after 1 day of exposure

to SBF. Only NaCl-rich plates with no evidence of P-containing compounds were observed by SEM-EDX.

Figures 8(a) and 8(b) show the concentration of ionic Si and P species, respectively, determined by ICP. These graphs represent the scaffold dissolution profiles as a function of soaking time in SBF. As Si species increase in the SBF (which originally did not contain any Si species) with increasing immersion time, P species are progressively removed from the solution. On the other hand, the as-fabricated scaffold had no P in its original composition, but, upon exposure to SBF, P is already detected by EDX on the surface and even at the fracture surface of the samples. X-ray diffraction measurements might be useful to identify the apatite formation on the sample; however, the calcium-phosphate layers formed at this stage were not thick enough to be detected by this technique. XPS results, not shown here, give a Ca/P ratio of 1.4 for the scaffold surface soaked for 1 day in SBF, which is lower than the 1.66 value of HA, but additional supporting evidence for the formation of HA is found from SEM analysis, which shows surface features formed at the samples as being very similar to those characteristic of apatite grains and layers.[15] Moreover, the exchange of Si species (from the sample) by P species (from the solution), observed upon immersion of the porous samples in SBF, agrees with the findings from Figs. 5 and 6 and with the typical HA formation steps reported in Ref. 19.

In vitro cell studies have been performed on the sol-gel samples prepared without PEO and, therefore, without macropores, but exhibiting different levels of nanoporosity. The aim at this stage is to establish the independent effect of high surface area and enlarged nanopores on the adhesion of osteoblast-like cells. Future experiments will be dedicated to understanding the effect of macropores on the cell attachment and proliferation. Figure 9 shows SEM images of the cells cultured on nanoporous sol-gel glass samples. The cells

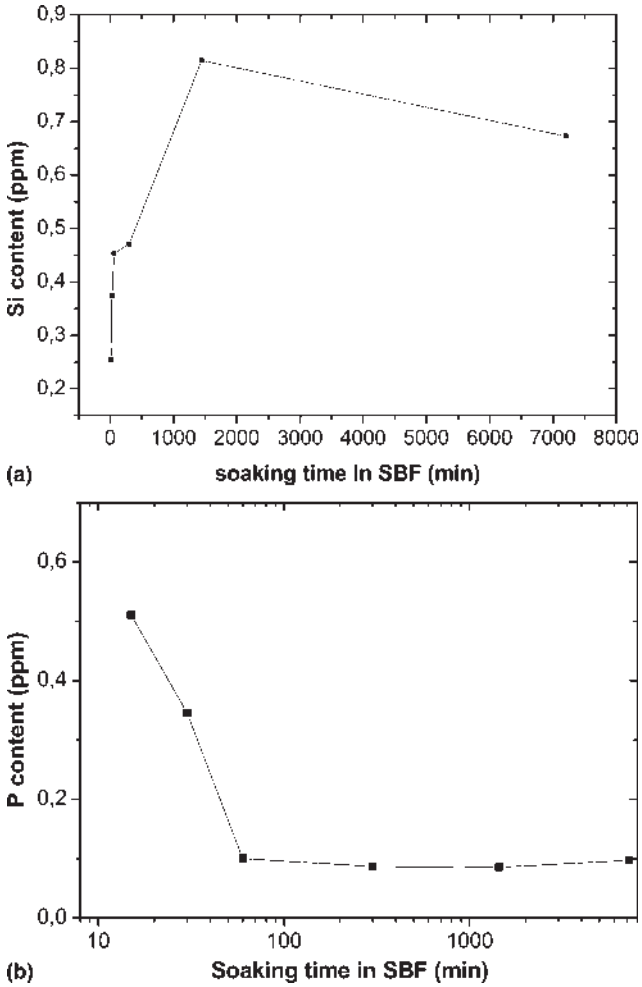

FIG. 8. Scaffold dissolution profiles with soaking in SBF: (a) Si content and (b) P content in SBF, as a function of soaking time.

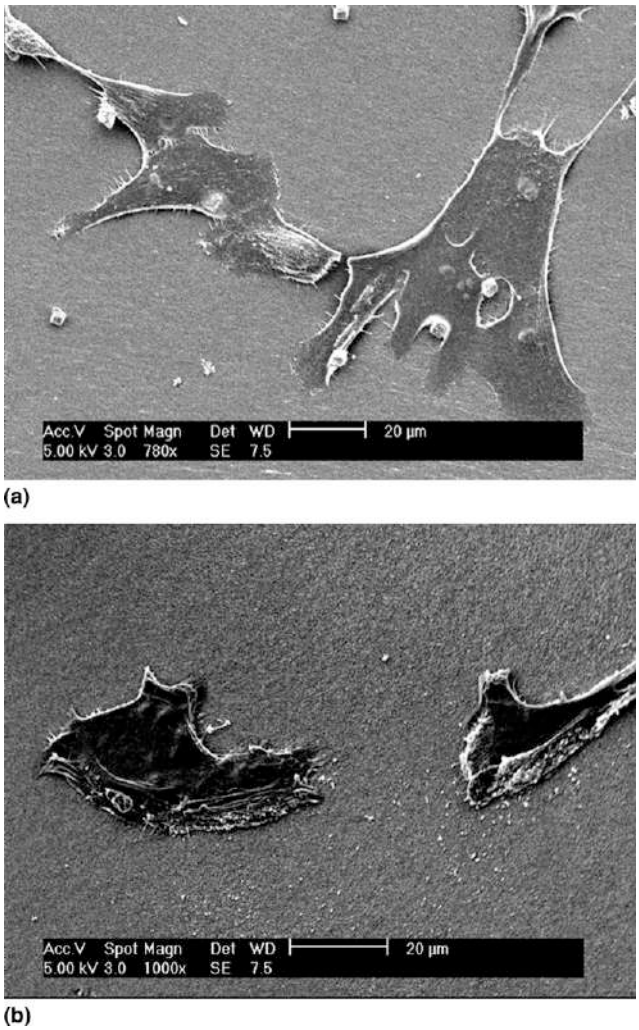

FIG. 9. SEM images of MG63 cells on sol-gel glasses (a) with solvent exchange process and, therefore, enlarged nanopores and (b) without solvent exchange process, therefore, with normal, smaller nanopores.

exhibit a well spread, flattened morphology and well-formed cell-to-cell contacts on enlarged nanoporous sol-gel glass with solvent exchange process [Fig. 9(a)], while cells on sol-gel glass without sol-gel exchange process, i.e., with smaller nanopores, are attached loosely [Fig. 9(b)]. These observations reveal that the cell attachment may be enhanced by enlarged nanopores by a simple process of solvent exchange in the gel state.

IV. CONCLUSIONS

Using a recently developed modified sol-gel method, the preparation and characterization of resorbable glass scaffolds with high pore interconnectivity and enhanced bioactivity are reported in this work. They consist of macropores of ~5 to 300 μm in size within a coral-like gel/glass skeleton, and nanopores ~5–20 nm in size, a desired porosity for rapid HA formation and bone cell in-growth and vascularization. The high pore interconnectivity, along with their high surface area and biocompatible composition, enhances bioactivity as demonstrated by the formation of hydroxyapatite deep inside the 3-D porous structure, and improved cell response. The macroporosity in this biomaterial is derived from the addition of a polymer to the sol, leading to phase separation of the gelling solution simultaneously with the sol-gel transition. Removal of the solvent-rich phase by evaporation and polymer burn-off introduces macroporosity. On the other hand, nanoporosity that is inherent to the sol-gel method, results mainly from the water/ethanol removal process. It can be further tailored by solvent exchange procedures demonstrated here.

ACKNOWLEDGMENTS

We would like to acknowledge the financial support of National Science Foundation through its International Materials Institute for New Functionality in Glass (IMI-NFG) at Lehigh University, and the Materials World Network program (Grant Nos. DMR-0409588, DMR-0844014, and DMR-0602975), and also a research scholarship from IST in Lisboa (Portugal). We are grateful to Prof. John DuPont and Dr. Timothy Anderson for help with the DTA/TGA analysis, Prof. Arup SenGupta and Dr. Sudipta Sarkar for help with the ICP measurements, and Ms. Erika Nelums for performing some of the Hg porosimetry measurements.

REFERENCES

1. J.R. Jones, L.M. Ehrenfried, and L.L. Hench: Optimizing bioactive glass scaffolds for bone tissue engineering. *Biomaterials* **27,** 964 (2006).
2. L.L. Hench, R.J. Splinter, W.C. Allen, and T.K. Greenlee, Jr.: Bonding mechanisms at the interface of ceramic prosthetic materials. *J. Biomed. Mater. Res.* **2,** 117 (1971).
3. M.M. Pereira and L.L. Hench: Mechanisms of hydroxyapatite formation on porous gel-silica substrates. *J. Sol-Gel Sci. Technol.* **7,** 59 (1996).
4. T.M. Freyman, I.V. Yannas, and L.J. Gibson: Cellular materials as porous scaffolds for tissue engineering. *Prog. Mater. Sci.* **46,** 273 (2001).
5. K. Nakanishi: Pore structure control of silica gels based on phase separation. *J. Porous Mater.* **4,** 67 (1997).
6. R. Takahashi, S. Sato, T. Sodesawa, T. Goto, K. Matsutani, and N. Mikami: Bending strength of silica gel with bimodal pores: Effect of variation in mesopore structure. *Mater. Res. Bull.* **40,** 1148 (2005).
7. P. Sepulveda, J.R. Jones, and L.L. Hench: Bioactive sol-gel foams for tissue repair. *J. Biomed. Mater. Res.* **59,** 340 (2002).
8. J.R. Jones, O. Tsigkou, E.E. Coates, M.M. Stevens, J.M. Polak, and L.L. Hench: Extracellular-matrix formation and mineralization on a phosphate-free porous bioactive glass scaffold using primary human osteoblast (HOB) cells. *Biomaterials* **28,** 1653 (2007).
9. H. Maekawa, J. Esquena, S. Bishop, C. Solans, and B.F. Chmelka: Meso/macroporous inorganic oxide monoliths from polymer foams. *Adv. Mater.* **15,** 591 (2003).
10. W. Liang and C. Russel: Resorbable, porous glass scaffolds by a salt sintering process. *J. Mater. Sci.* **41,** 3787 (2006).
11. H.S. Yun, S.E. Kim, and Y.T. Hyun: Fabrication of hierarchically porous bioactive glass ceramics. *Key Eng. Mater.* **361–363,** 285 (2008).
12. C.M. Lofton, C.B. Milz, H. Huang, and W.M. Sigmund: Bicontinuous porosity in ceramics utilizing polymer spinodal phase separation. *J. Eur. Ceram. Soc.* **25,** 883 (2005).
13. A.C. Marques, H. Jain, and R.M. Almeida: Sol-gel derived nano/macroporous monolithic scaffolds. *Phys. Chem. Glasses: Eur. J. Glass Sci. Technol. B* **48,** 65 (2007).
14. A.C. Marques, H. Jain, and R.M. Almeida: Nano/macroporous monolithic scaffolds prepared by the sol-gel method. *J. Sol-Gel Sci. Technol.* **51,** 42 (2009).
15. T. Kokubo and H. Takadama: How useful is SBF in predicting in vivo bone bioactivity? *Biomaterials* **27,** 2907 (2006).
16. R.M. Almeida and A.C. Marques: Characterization of sol-gel materials by infrared spectroscopy, in *Handbook of Sol-Gel Science and Technology*, edited by S. Sakka (Kluwer Academic Publishers, London, 2005).
17. M.M. Pereira, A.E. Clark, and L.L. Hench: Calcium phosphate formation on sol-gel-derived bioactive glasses in vitro. *J. Biomed. Mater. Res.* **28,** 693 (1994).
18. N. Olmo, A.I. Martín, A.J. Salinas, J. Turnay, M. Vallet-Regi, and M.A. Lizarbe: Bioactive sol-gel glasses with and without a HCA layer as substrates for osteoblast cells adhesion and proliferation. *Biomaterials* **24,** 3383 (2003).
19. J. Zhong and D.C. Greenspan: Processing and properties of sol-gel bioactive glasses. *J. Biomed. Mater. Res.* **53,** 694 (2000).